*minerals*

MDPI

*Article*

# Petrogenesis of Early Triassic Felsic Volcanic Rocks in the East Kunlun Orogen, Northern Tibet: Implications for the Paleo-Tethyan Tectonic and Crustal Evolution

**Dongdong Yan [1,2], Zhiqiang Chu [1], Zhongyuan Liu [1], Wei Wang [1] and Fuhao Xiong [1,3,*]**

[1] College of Earth Science, Chengdu University of Technology, Chengdu 610059, China; ydd19961129@163.com (D.Y.); 15899435233@163.com (Z.C.); liuzhongyuan43@hotmail.com (Z.L.); weiwang20221010@163.com (W.W.)
[2] Key Laboratory of Tectonic Controls on Mineralization and Hydrocarbon Accumulation, Chengdu University of Technology, Chengdu 610059, China
[3] State Key Laboratory of Oil and Gas Reservoir Geology and Exploitation, Chengdu University of Technology, Chengdu 610059, China
* Correspondence: fhxiong@cdut.edu.cn

**Abstract:** The felsic volcanic rocks in orogenic belts are vital probes to understand the tectonic evolution and continental crust growth. Here, we present a comprehensive study on the zircon U–Pb geochronology, whole-rock geochemistry, and zircon Lu-Hf isotopes of Early felsic volcanic rocks from the Hongshuichuan Formation, East Kunlun Orogen, Northern Tibet, aiming to explore their petrogenesis and implications for the Paleo-Tethyan orogeny and crustal evolution. The studied felsic volcanics comprise rhyolite porphyry and rhyolite, exhibiting coeval zircon U–Pb ages of ca. 247–251 Ma. Rhyolite porphyries show metaluminous to peraluminous nature (A/CNK = 0.88–1.24) with high $SiO_2$ contents (72.1–78.9 wt%) and moderate $Mg^{\#}$ values (22–40), and they display enrichment of LREE with $(La/Yb)_N$ ratios of 6.02–17.9 and depletion of high field strength elements. In comparison, the rhyolites are strongly peraluminous (A/CNK = 1.09–1.74) with high $SiO_2$ contents (71.7–74.3 wt%) and high $Mg^{\#}$ values (43–52) and are also enriched in LREE ($(La/Yb)_N$ of 6.65–18.4) and depleted in HFSE (e.g., Nb, Ta, Ti). Combining with their different zircon Lu-Hf isotopes, i.e., enriched isotopes for the rhyolite porphyries ($\varepsilon Hf(t) = -7.3$ to $-3.8$) and depleted Hf isotopes for the rhyolites ($\varepsilon Hf = -0.6$ to $+3.0$), we interpret that the studied rhyolite porphyries and rhyolites were derived by partial melting of Mesoproterozoic metagreywacke sources followed by plagioclase-dominated fractional crystallization, but the latter shows the significant contribution of crust–mantle magma mixing. The mixed mantle-derived magma comes from an enriched lithospheric mantle source that had been metasomatized by subduction-related fluids. Combining with other geological evidence, we propose that the studied Early Triassic felsic volcanic rocks were formed in a subduction arc setting, and the reworking of ancient continental crust with crust–mantle magma mixing is the major mechanism of crustal evolution in the East Kunlun Paleo-Tethyan orogenic belt.

**Keywords:** East Kunlun; felsic volcanic rocks; Early Triassic; Paleo-Tethyan; tectonic setting

check for updates

**Citation:** Yan, D.; Chu, Z.; Liu, Z.; Wang, W.; Xiong, F. Petrogenesis of Early Triassic Felsic Volcanic Rocks in the East Kunlun Orogen, Northern Tibet: Implications for the Paleo-Tethyan Tectonic and Crustal Evolution. *Minerals* **2023**, *13*, 607. https://doi.org/10.3390/min13050607

Academic Editor: Alexey V. Ivanov

Received: 23 March 2023
Revised: 24 April 2023
Accepted: 25 April 2023
Published: 27 April 2023

**Copyright:** © 2023 by the authors. Licensee MDPI, Basel, Switzerland. This article is an open access article distributed under the terms and conditions of the Creative Commons Attribution (CC BY) license (https://creativecommons.org/licenses/by/4.0/).

## 1. Introduction

As the most archetypal products of a long-lived orogeny, felsic volcanics record the continental crust growth and tectonic evolution of Paleo-orogenic belts [1–3]. Several petrogenetic models have been proposed for the origin of felsic volcanic rocks in orogenic belts: (1) advanced degrees of fractional crystallization of mantle-derived mafic magmas [4,5], (2) partial melting of continental crust triggered by the underplating of mantle-derived mafic magmas [6–8], and (3) hybridization of crustal felsic melts with mantle-derived mafic melts [9–12]. Thus, identifying the petrogenesis of felsic volcanics is the key to reveal the mechanism of crust–mantle interaction as well as continental evolution and tectonic history of Paleo-orogenic belts.

The East Kunlun Orogen Belt (EKOB), one typical tectonic-magmatic belt in the northern Tibet Plateau, has experienced Paleo-Tethyan subduction collision orogeny as recorded by large-scale Permian-Triassic felsic magmatism. Although much research has been carried out on the Paleo-Tethyan felsic magmatism in the EKOB, its petrogenesis and geodynamic background are still controversial. Some studies propose that most Early to Middle Triassic felsic volcanics are formed in a subduction setting and the Kunlun Paleo-Tethyan ocean was finally closed in Late Triassic, while other studies emphasize that the Kunlun Paleo-Tethyan ocean was closed in Late Permian, and the Triassic felsic volcanics all are generated in a post-collisional setting. Meanwhile, some scholars even proposed that the Paleo-Tethyan oceanic subduction lasted until the Late Triassic or Jurassic [2,13–15]. Due to the rare occurrence of Early Triassic felsic volcanic rocks in the EKOB, previous studies mainly focus on the large-scale developed Late Triassic volcanic rocks, including abundant andesitic to rhyolitic lavas and volcaniclastic rocks [16,17]. However, the petrogenesis and geodynamic background of the Early Triassic felsic volcanic magmatism in the EKOB are still unclear, which restricts our understanding of the East Kunlun Paleo-Tethyan orogeny.

Herein, we carried out systematic studies on zircon U-Pb ages, bulk-rock major and trace element compositions, and zircon Lu-Hf isotopes of Early Triassic felsic volcanic rocks in the EKOB to discuss their petrogenesis. These data, as well as the published dataset of the Late Triassic felsic rocks, help us reveal the tectonic setting of the Early Triassic data for volcanic rocks and reconstruct the tectonic and crustal evolutionary history of the East Kunlun Paleo-Tethyan orogen.

## 2. Regional Geologic Background

The EKOB is located in the northern Tibet Plateau, NW China, adjoins the Qaidam block in the north, the Bayan Har Orogen in the south, and the West Qinling Orogen in the east (Figure 1a). The orogen extends for nearly 1500 km from east to west along the northern margin of the Tibetan Plateau, with a width between 50 km and 200 km. Based on the central and south Kunlun faults, the EKOB can be divided into the Northeast Kunlun terrane and the Southeast Kunlun terrane. Due to Paleo-Tethyan oceanic subduction and subsequent collision, large–scale Late Permian to Triassic felsic magmatism occurred in the EKOB (Figure 1b) [2,14]. Permian-Triassic felsic intrusive rocks are dominated by granites and granodiorites with abundant mafic magmatic enclaves [13,18–21], while the felsic volcanic rocks are mainly Late Triassic in age (e.g., Elashan Formation) [17], with smaller volumes of Late Permian to Early Triassic age [22].

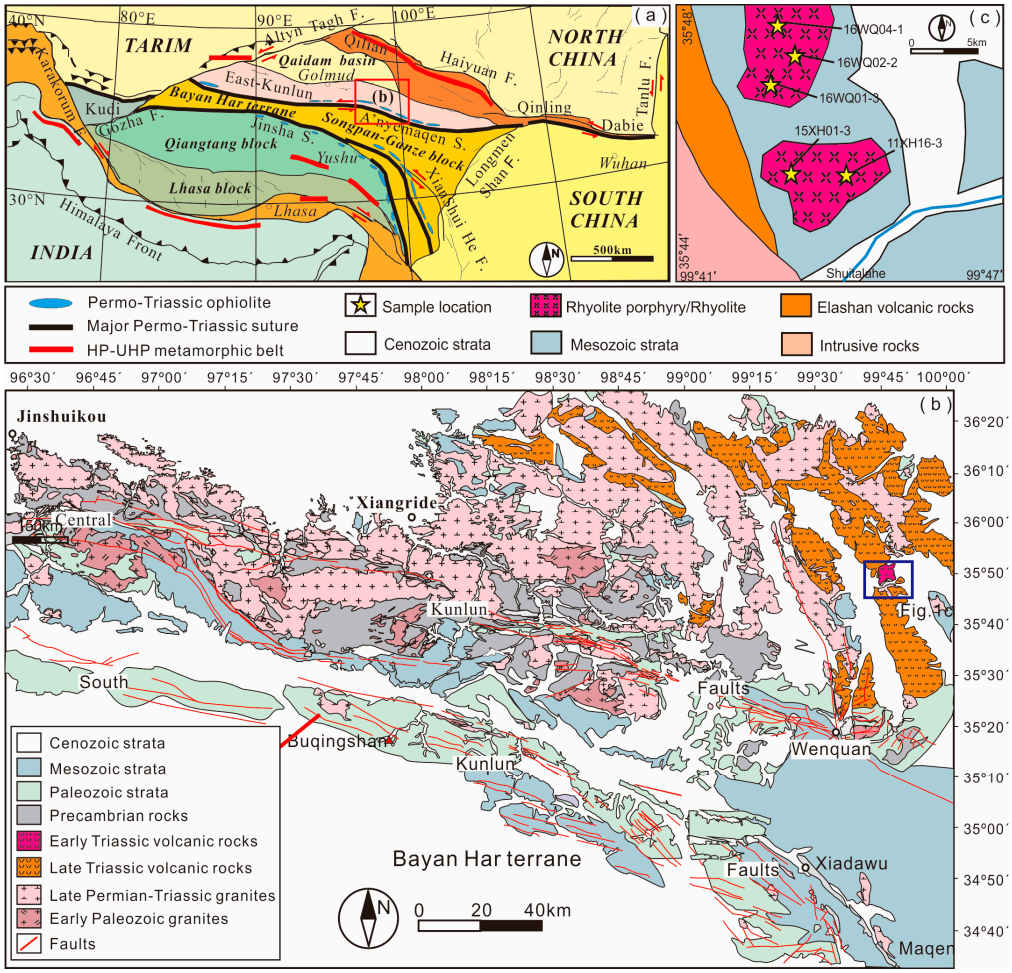



**Figure 1.** (**a**) Tectonic outline of the Tibetan Plateau (modified after [23]); (**b**) simplified geological map of the eastern section of East Kunlun showing the distribution of Permian-Triassic granites (modified after [14]); and (**c**) simplified distribution map of the Hongshuichuan volcanics, showing the studied sample's location.

The crustal basement of the EKOB is represented by the Paleo- and Mesoproterozoic Jinshuikou Group comprising the lower Baishahe and upper Xiaomiao formations. The lower Baishahe Formation consists of marbles, gneisses, migmatites, and amphibolites. The upper Xiaomiao Formation comprises marbles, gneisses, greenschists, and quartzites [24–27]. The basement is covered by the Permian-Triassic volcanic-sedimentary strata, such as the Late Permian Gequ Formation, the Early Triassic Hongshuichuan Formation, and the Middle Triassic Naocangjiangou Formation. Among them, the Early Triassic Hongshuichuan Formation is mainly composed of quartz sandstone, bioclastic limestone, lavas, and pyroclastic rocks. This set of strata is mainly composed of limestone and sandstone; lavas mainly occur in it in the form of volcanic strata in different stratigraphic units of the Hongshui Chuan Formation, which is the product of a marine eruptive environment. The volcanic lavas in this study are sampled from the Hongshuichuan Formation, which mainly comprises rhyolite and rhyolite porphyry and is interbedded with contemporaneous early Mesozoic sedimentary strata (Figure 1c).

## 3. Sampling and Petrography

The Early Triassic felsic volcanic rocks in the Hongshuichuan Formation overlie limestone. Rhyolite is located above rhyolite porphyry and is separated by quartz sandstone and bioclastic limestone. The rhyolite porphyries are greyish-green and have spherulitic or porphyritic texture (Figure 2c). The phenocrysts are K-feldspar (20–25 vol%), quartz

(5–10 vol%), plagioclase (5–10 vol%), and biotite (3–5 vol%), and the groundmass shows an aphanitic texture and constitutes feldspar and quartz microlite (Figure 2g,h). The plagioclase phenocrysts can be classified as oligoclase-andesine ($An_{28–32}$). Accessory minerals mainly include titanite, rutile, zircon, apatite, and ilmenite. The rhyolites are gray and exhibit porphyritic texture with phenocrysts of K-feldspar (15–20 vol%), quartz (10–15 vol%), and minor plagioclase (5–10 vol%), and aphanitic matrix of subhedral quartz and feldspar (Figure 2e,f). All the plagioclase phenocrysts are andesine in composition ($An_{31–38}$). Accessory minerals include magnetite, zircon, apatite, and rutile. Different from rhyolite porphyry, most plagioclase phenocrysts of the rhyolites show zoning texture, indicating that there is magma mixing in the formation of rhyolite.

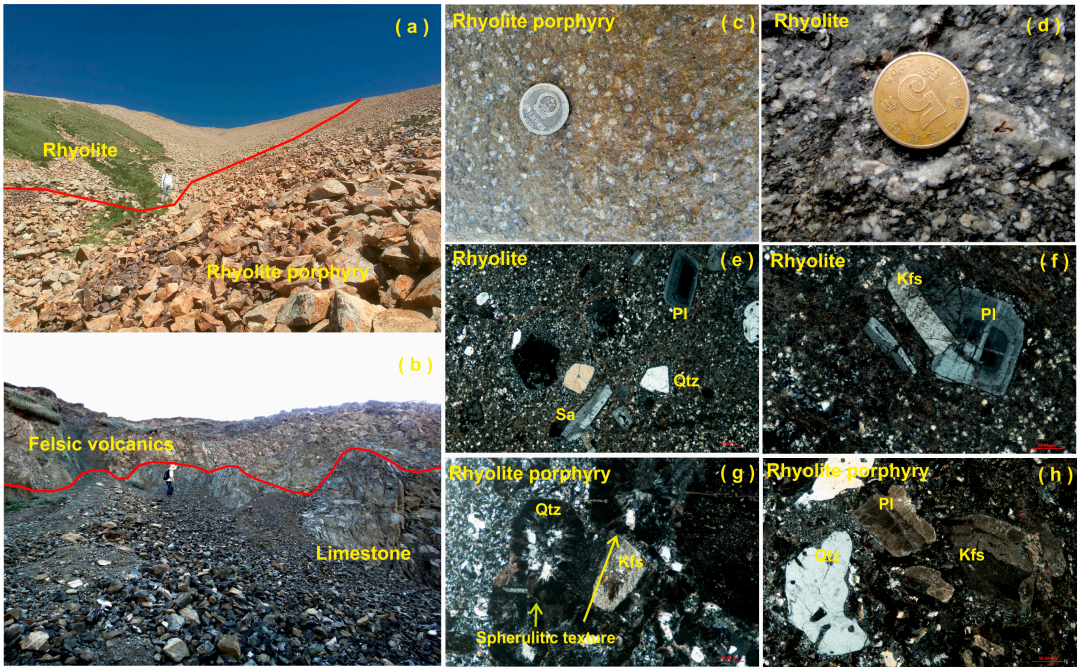



**Figure 2.** Field and microscope graphics of the Hongshuichuan volcanics in East Kunlun. (**a**,**b**) Field photographs of the felsic volcanics; (**c**) rhyolite porphyry; (**d**) rhyolite; (**e**,**f**) microphotographs of the rhyolite; and (**g**,**h**) microphotographs of the rhyolite porphyry. Mineral abbreviations: Kfs, K-feldspar; Pl, plagioclase; Qtz, quartz; Sa, sanidine.

## 4. Analytical Methods

### *4.1. LA-ICP-MS Zircon U-Pb Dating*

The studied samples were collected from fresh outcrops and zircons were separated by heavy liquid and magnetic methods. Zircon grains were photographed with an optical microscope and the internal structures were analyzed by cathodoluminescence (CL). Zircon U-Pb isotope and trace element concentration were determined using a 193 nm Geo Las Pro and an Agilent 7500a ICP-MS with a laser spot beam of 32 μm at the State Key Laboratory of Geological Processes and Mineral Resources (GPMR), China University of Geosciences, Wuhan. For the external standards and calibration of mass discrimination and isotope fractionation, zircon 91,500 and zircon GJ-1 were used, respectively. A background acquisition time of 18–20 s and a data acquisition time of 50 s was adopted for each measurement. Helium was applied as a carrier gas, and Ar was used as the makeup gas and mixed with the carrier gas via a T-connector before entering the ICP source. Nitrogen was added to the central gas flow (Ar + He) of the Ar plasma to lower the detection limits and improve precision. Concordia diagrams and weighted mean ages were made by Isoplot/Ex_ver3 [28]. Data were processed using ICPMSDataCal [29]. The detailed operating conditions for the laser system and ICP-MS instrument are described by Liu et al. [29].

### *4.2. Whole-Rock Major and Trace Element Analyses*

Whole-rock samples were crushed in a corundum jaw crusher (to 60 mesh). About 60 g of this material was powdered in an agate ring mill to <200 mesh for whole-rock geochemical analysis. The major element analysis was conducted by standard X-ray fluorescence (XRF) methods, using a Shimadzu Sequential 1800 spectrometer at the GPMR. Precision is <3% and accuracy is <4% for the major elements. The detailed techniques for major element analysis were described by Ma et al. [30]. The trace element compositions were determined using an Agilent 7700a ICP-MS with analytical precision ranging from 5 to 10%. The samples were digested by HF +$HNO_3$ in Teflon bombs. Analyses of USGS standards (AGV–2, BHVO–2, BCR–2 and RGM–2) indicate accuracy better than 5%–10% for most trac elements. The analysis was conducted using ICP-MS (Agilent 7700) and ICP–AES (Agilent VISIA) methods after the rock powder (200 mesh) had been dissolved by HF–$HNO_3$–$HClO_4$–HCl acid digestion. The relative standard deviation of the elemental concentrations is close to or below 10%. The sample digestion procedures and ICP-MS methods are as described by Liu et al. [31].

### *4.3. Zircon Lu-Hf Isotope Analyses*

In-situ Lu-Hf isotope analysis was conducted at the State Key Laboratory of GPMR, China, using a Neptune Plus MC-ICP-MS equipped with a Geolas 193 nm ArF Laser Ablation System (LAS). Measurement was completed on the ablation spots close to those for the U-Pb dating with a spot beam of 44 μm. Acquisition of background and ablation signals were completed for 20 s and 50 s, respectively. Detailed operating conditions for the laser ablation system and the MC-ICP-MS instrument and analytical method are the same as described by Hu et al. [32]. Off-line selection and integration of analytical signals and mass bias calibrations were performed using ICPMSDataCal [31].

## 5. Results

### *5.1. Zircon U–Pb Ages and Trace Elements*

#### 5.1.1. Zircon U–Pb Ages

Representative CL images of analyzed zircons and corresponding Concordia diagrams are shown in Figures 3 and 4, respectively. The age data are given in Table S1. Most of the zircon grains are euhedral to subhedral, ranging in size from 100 to 300 μm. They are characterized by oscillatory magmatic zoning (Figure 3).




**Figure 3.** Cathodoluminescence images of representative zircons from the rhyolite ((**a**,**b**) 15XH01−3; 11XH16−3), rhyolite porphyry ((**c**–**e**) 16WQ04−1; 16WQ02−2; 16WQ01−3) of the Hongshuichuan volcanic rocks. The circles are analysis spots of zircon U−Pb dating, indicating their ages (Ma).

Fourteen zircon grains of rhyolite (15XH01-3) yield low Th/U ratios (0.58–1.25), diagnostic of magmatic origin [33]. The concordant crystals of rhyolite yield a weighted mean $^{206}Pb/^{238}U$ age of 250.4 ± 2.0 Ma (1 s, MSWD = 1.4) (Figure 4a,b). Fourteen zircons from rhyolite 11XH16–3 form a tight cluster with a weighted mean $^{206}Pb/^{238}U$ age of 251.7 ± 1.6 Ma (1 s, MSWD = 1.19), with low Th/U ratios (0.59–0.96) (Figure 4c,d).

Fifteen zircon crystals of rhyolite porphyry (16WQ04–1) yield a weighted mean $^{206}Pb/^{238}U$ age of 248.1 ± 2.6 Ma (1 s, MSWD = 1.4), with low Th/U ratios (0.55–0.76), which are typical of magmatic zircons (Figure 4e,f). The rhyolite porphyry (16WQ02-2), with a low Th/U ratio (0.39–0.86), yield a weighted-mean $^{206}Pb/^{238}U$ age of 247.9 ± 2.4 Ma (1 s, MSWD = 1.8) (Figure 4g,h) based on nineteen analyzed zircon spots. Nineteen crystals from rhyolite porphyry 16WQ01–3 give a weighted mean $^{206}Pb/^{238}U$ age of 249.7 ± 2.0 Ma (1 s, MSWD = 1.9). The zircon crystals have low Th/U ratios of 0.34 to 0.57 (Figure 4i,j). Thus, the above results indicate the studied rhyolite and rhyolite porphyry have identical crystallization ages of ca. 251–247 Ma.

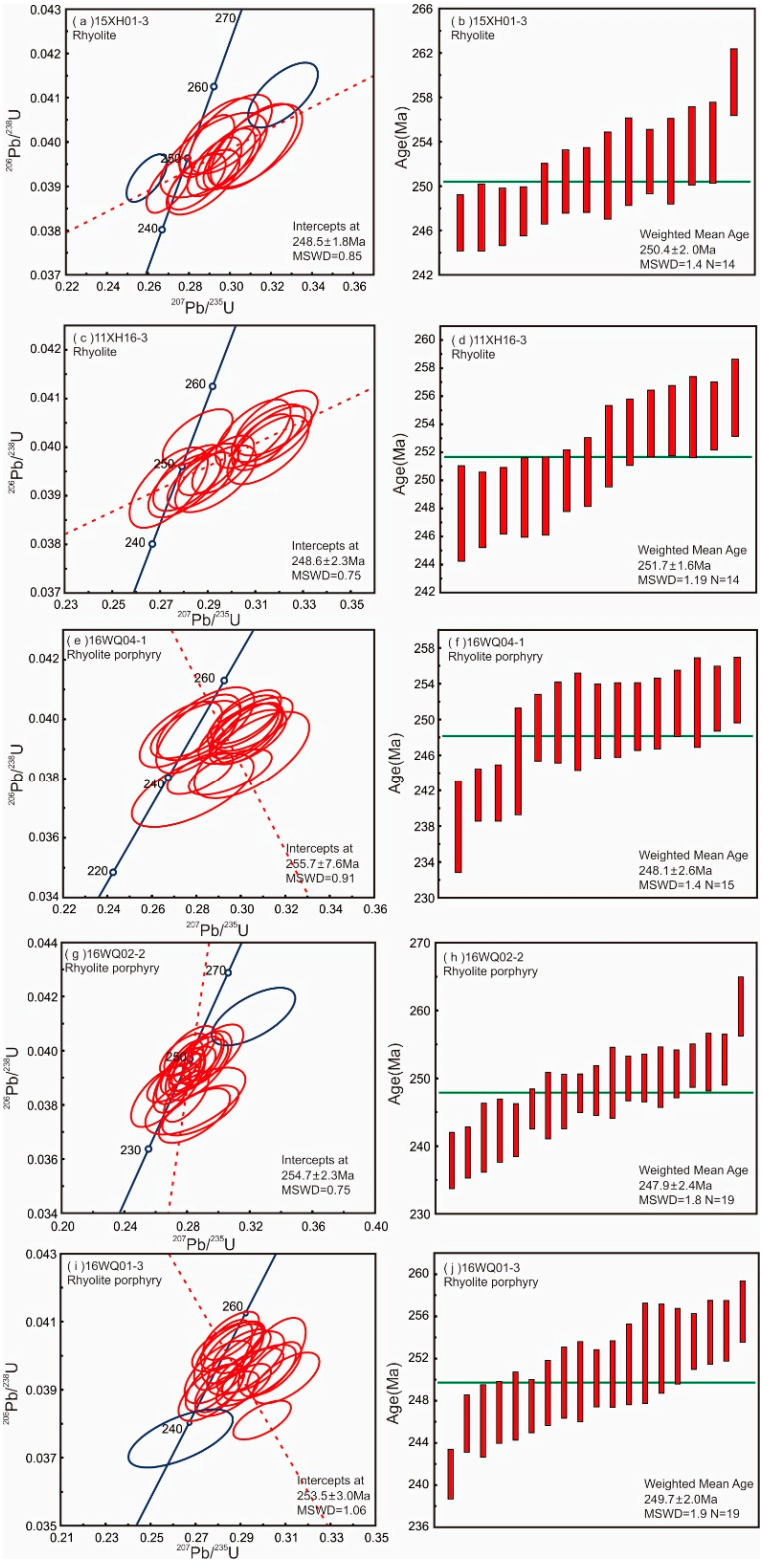



**Figure 4.** Wetherill Concordia diagrams and weighted mean $^{206}Pb/^{238}U$ age for zircons from the Hongshuichuan volcanics. (**a**,**b**) 15XH01−3 rhyolite; (**c**,**d**) 11XH16−3 rhyolite; (**e**,**f**) 16WQ04−1 rhyolite porphyry; (**g**,**h**) 16WQ02−2 rhyolite porphyry; (**i**,**j**) 16WQ01−3 rhyolite porphyry. The blue circles represent points with large errors.

5.1.2. Zircon Trace Elements

The data for zircon trace elements are shown in Table S2. As shown in a chondrite-normalized REE plot, all analyses are LREE depleted and HREE enriched and show positive Ce and negative Eu anomalies, chemically identical to typical magmatic zircons (Figure 5a) [34]. Zircons from rhyolite contain higher Hf (~9066 ppm), Th/U (~0.91), Yb/Gd (~21.09), Eu/Eu* (~0.26), and U/Yb (~1.18) and lower REE contents (~1383 ppm) than those from rhyolite porphyry (Hf = ~8898 ppm; Th/U = ~0.57; Yb/Gd = ~16.24; Eu/Eu* = ~0.14; U/Yb = ~0.92; REE = ~1416 ppm), which may reflect their different origins.

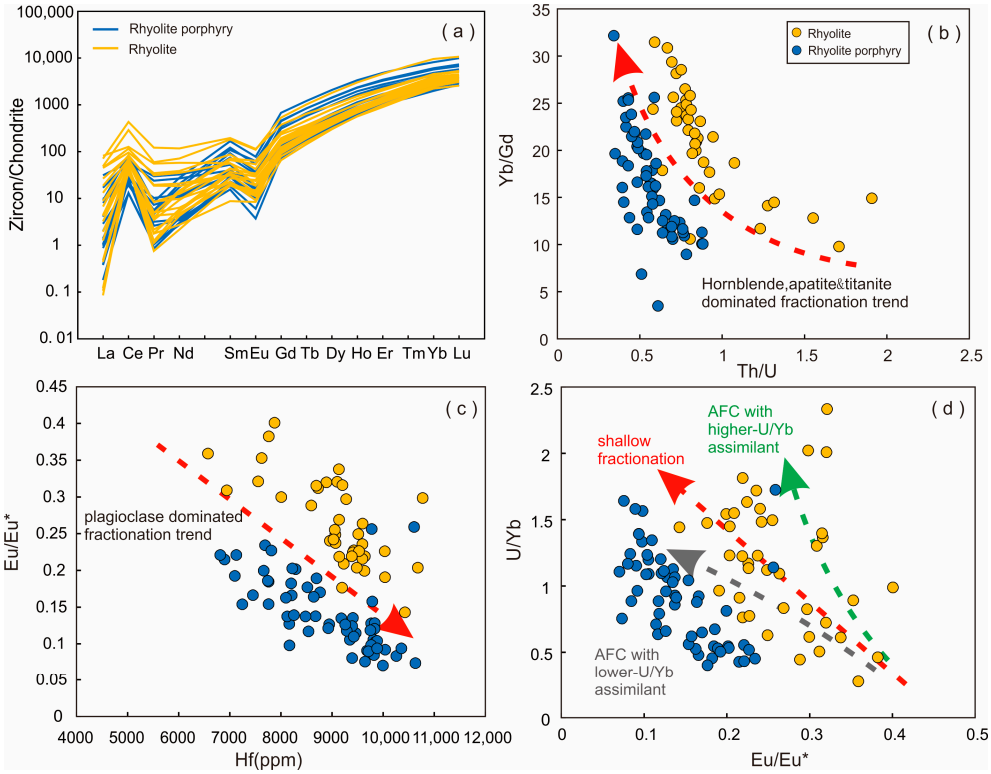



**Figure 5.** (**a**) Chondrite-normalized REE patterns of zircons from the Hongshuichuan volcanics and (**b**–**d**) variations in selected trace elements for zircons from the Hongshuichuan volcanics.

*5.2. Whole-Rock Geochemistry*

Whole-rock major and trace element analyses are given in Table S3. The rhyolite porphyry and rhyolites are highly differentiated felsic rocks ($SiO_2$ = 72.1–78.9 wt% and $SiO_2$ = 71.7–74.3 wt%, respectively). They all plot in the sub-alkaline rhyolite field on the Total Alkali-Silica (TAS) diagram (Figure 6a). The rhyolite porphyry has a wide range of $K_2O$ contents (1.20–7.17 wt%), high contents of total alkaline ($Na_2O + K_2O$ = 5.76–8.79 wt%), and moderate $Al_2O_3$ (10.8–14.9 wt%), $FeO^T$ (1.50–2.33 wt%), and $Mg^{\#}$ (22–40). They are weakly peraluminous (A/CNK = 0.88–1.24; molar $Al_2O_3/(CaO + Na_2O + K_2O)$) (Figure 6d). The rhyolite defines a high-K calc-alkaline trend and total alkaline ($Na_2O + K_2O$ = 6.09–7.77 wt%) and moderate contents of $Al_2O_3$ (12.7–16.0 wt%) and $FeO^T$ (1.49–2.26 wt%) (Figure 6b). The rhyolite samples are peraluminous with A/CNK values of 1.09–1.74 and exhibit high $Mg^{\#}$ values (43–52).

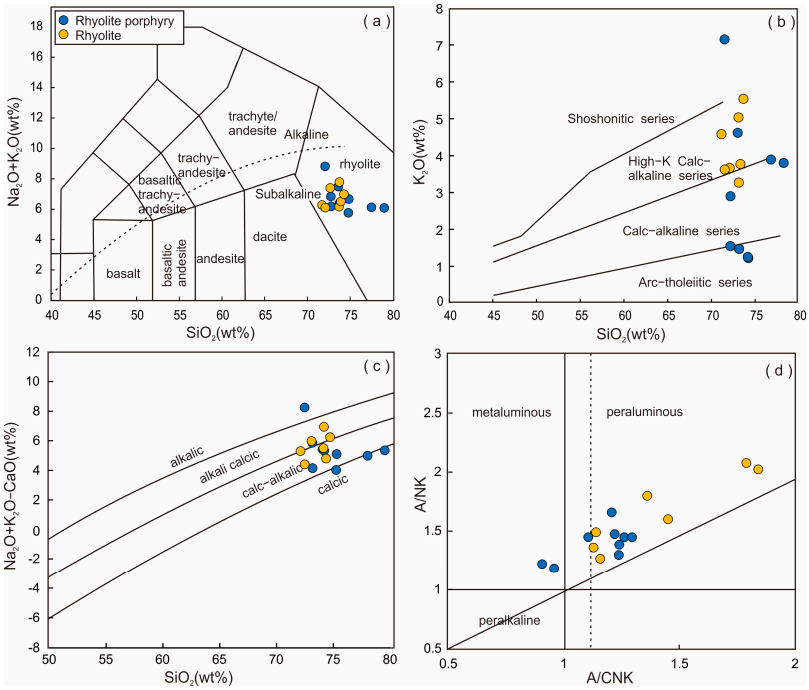



**Figure 6.** Geochemical classification of the Hongshuichuan volcanics. (**a**) Total alkali vs. silica (TAS) diagram after [35]; (**b**) $K_2O$ vs. $SiO_2$ diagram after [36]; (**c**) ($Na_2O + K_2O - CaO$) vs. $SiO_2$ diagram (after [37]); and (**d**) alumina saturation index shown by A/CNK vs. A/NK diagram (after [36]).

The rhyolite porphyries and rhyolites are characterized by the enrichment of light rare earth elements (LREEs) and the depletion of heavy rare earth elements (HREEs) ($(La/Yb)_N$ = 6.02–17.9 and 6.65–18.4, respectively). They all display negative Eu anomalies (Eu/Eu* = 0.51–0.65 and 0.39–0.70, respectively), probably indicative of plagioclase fractionation (Figure 7a). The rhyolite porphyries and rhyolites exhibit similar trace element patterns, exhibiting overall enrichment of large ion lithophile elements (LILE; e.g., Th, Rb, and Ba) and LREE and depletion of high field strength elements (HFSE; e.g., Nb, Ta, Ti, and P; Figure 7b).

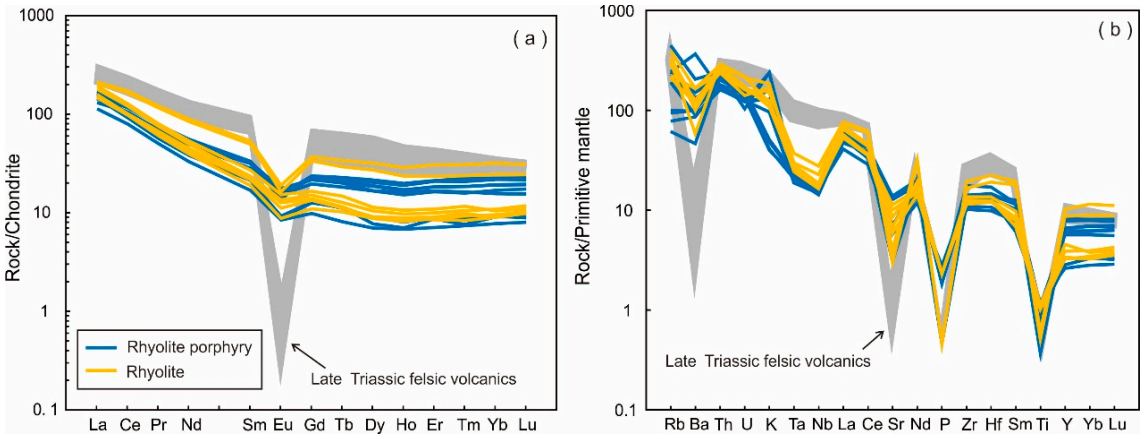



**Figure 7.** (**a**) chondrite-normalized REE distribution of the studied Hongshuichuan volcanics; (**b**) primitive-mantle-normalized trace element spider diagram of studied Hongshuichuan volcanics. Normalized values for the primitive-mantle and chondrite REE diagrams were taken from [38] and [39], respectively. Data sources: [11,16,17,40] and our unpublished results.

### *5.3. Zircon Lu-Hf Isotope*

Zircon Lu–Hf isotopic data are shown in Table S4. Ten zircon grains of rhyolite porphyry (16WQ02-2) exhibit $^{176}Hf/^{177}Hf$ ratios of 0.28242 to 0.28252 with significant negative εHf values (−7.3 to −3.8) and Mesoproterozoic crustal model ages ($T_{DM2}$ = 1448 to 1648 Ma) (Figure 8).

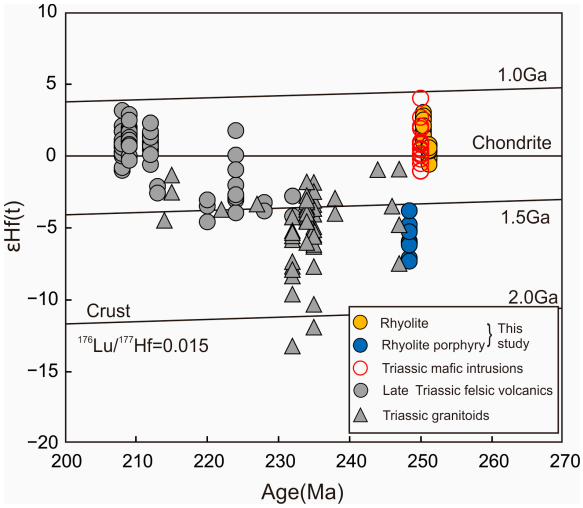



**Figure 8.** Zircon εHf(t) versus age diagram. Data sources are as follows: Triassic mafic intrusions are from [41]; Late Triassic felsic volcanics are from [11,16,17]; Triassic granitoids are from [42,43].

Fourteen zircon grains of rhyolite (15XH01-3) yield $^{176}Hf/^{177}Hf$ ratios varying from 0.28265 to 0.28271. They show positive εHf values (0.9 to 3.0), with Mesoproterozoic crustal model ages ($T_{DM2}$ = 1068 to 1187 Ma). Twelve analyzed zircon grains of rhyolite (11XH16-3) display $^{176}Hf/^{177}Hf$ ratios from 0.28261 to 0.28265 and yield weakly juvenile εHf values (−0.6 to 0.8), depicting Mesoproterozoic crustal model ages ($T_{DM2}$) from 1196 to 1266 Ma.

## 6. Discussion

### *6.1. Petrogenetic Type of the Felsic Volcanic Rocks*

Granitoids and their eruptive equivalents are usually divided into I-, S-, M-, and A-type granitic rocks based on their petrogenetic mechanisms. In general, I-type granitic rocks are usually derived by the crust–mantle interaction or partial melting of metamorphic igneous rocks [14,44], S-type granitic rocks are formed by melting of aluminum-rich metasedimentary rocks associated with collision or post-collision setting [45], M-type granitic rocks are mainly derived by fractional crystallization of mantle-derived magma, while A-type granitic rocks mainly originated from various magma sources in extensional environment [16]. Revealing the petrogenetic types of granitoids and their volcanic equivalents is the key to understanding their petrogenesis and geodynamic implications. Based on petrography and geochemical studies, we propose that the rhyolite and rhyolite porphyry are I-type granitic rocks. The critical supporting evidence is as follows:

Firstly, the studied rhyolite and rhyolite porphyry all display low Ce and HFSEs (Zr + Nb + Y + Ce) contents, low Ga/Al and $FeO^T/MgO$ ratios, contrary to the Late Triassic felsic volcanics, and all plot in the I-type granitic field according to various chemical classification diagrams (Figure 9a,b) [46]. This identification is also corroborated by the anti-correlation between $SiO_2$ and $Al_2O_3$ contents (Figure 9c,d). Additionally, the rhyolite and rhyolite porphyry show higher CaO contents (average of 1.11 wt% and 1.28 wt%) relative to the A-type granitic rocks (0.75 wt%) but closely match the I-type granitic rocks (1.71 wt%, [46–48]).

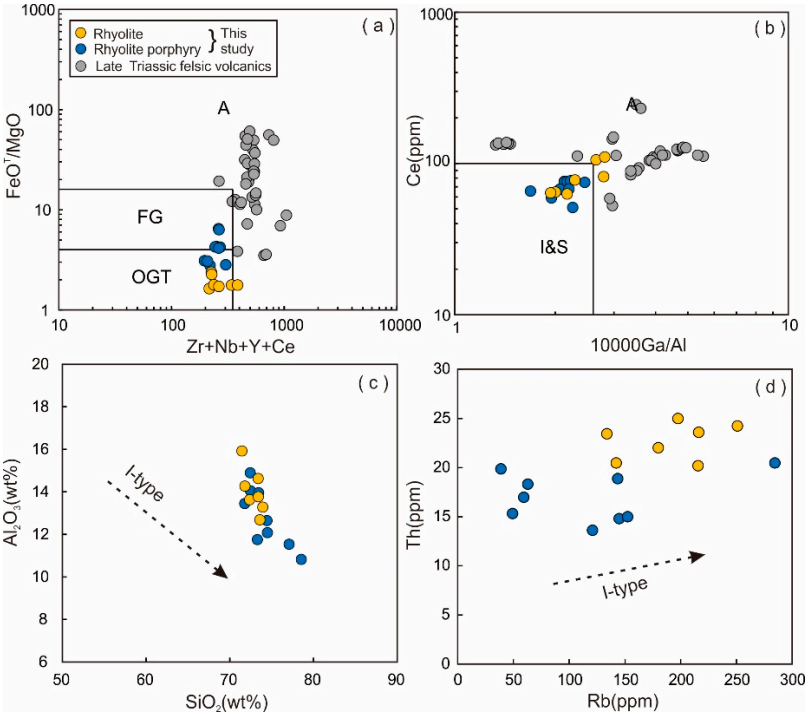



**Figure 9.** (**a**,**b**) Chemical discrimination diagrams (after [46]); (**c**) $SiO_2$ versus $Al_2O_3$; (**d**) Rb versus Th. Data sources: [11,16,17,40] and our unpublished results.

### *6.2. Origin of the Felsic Volcanic Rocks*

The studied rhyolite exhibits higher whole-rock $Mg^{\#}$ values (43–53) and zircon εHf values (−0.6 to 3.0) than the coeval rhyolite porphyry ($Mg^{\#}$ = 22–40; εHf = −7.3 to −3.8), implying their different origins or magmatic evolutionary processes.

The studied rhyolite porphyry has high contents of $SiO_2$, low contents of MgO, $TiO_2$, and $FeO^T$, and shows enrichment of large ion lithophile elements (Rb, Th, U, and K) and depletion of high field strength elements (Nb, Ta, Zr, and Hf) with remarkable depletion of Sr and Eu (Figure 10), which are typical features of crustal origin. In addition, the $K_2O$ value of rhyolite porphyry varies widely, which we believe is due to the hydration of glass [49]. The rhyolite may have undergone weathering after its formation. This is likely to lead to alter in the original glass matrix, and most samples absorbed K and lost Na. The ratios of incompatible trace elements (e.g., Th/Nb, Th/La, La/Nb, and Nb/Ta) usually remain constant during magma differentiation; thus, they are reflective of the nature of magma sources [50]. The average ratios of incompatible trace elements for the studied rhyolite porphyry (e.g., Th/Nb = 1.47; Th/La = 0.47; La/Nb = 3.21; Nb/Ta = 12.4) are higher than those of the primitive mantle (Th/Nb = 0.18; Th/La = 0.13; La/Nb = 0.94; Nb/Ta = 16.0) but closely identical to the average ratios of the continental crust (Th/Nb = 0.44; Th/La = 0.20; La/Nb = 2.20; Nb/Ta = 11.0–12.0) [51,52]. In addition, the studied rhyolite porphyry exhibits elemental geochemistry identical to those derived from pure crustal melting in a normal arc setting (Figure 11a,b). The rhyolite porphyry has high values of $Al_2O_3/(FeO_{tot} + MgO)$ and $CaO/(MgO + FeO_{tot})$, which is consistent with the melt derived from the metagreywacke source as expected by the experimental petrology (Figure 11c,d). Isotopically, their negative zircon εHf(t) values (−7.3 to −3.8) are significantly lower than those of the mantle-derived rocks or the juvenile crustal rocks (Figure 8). These lines of evidence, in combination with their Mesoproterozoic two-stage Hf model ages (1.4–1.6 Ga), suggest that the rhyolite porphyry was derived by partial melting of a Mesoproterozoic metagreywacke source in the lower crust.

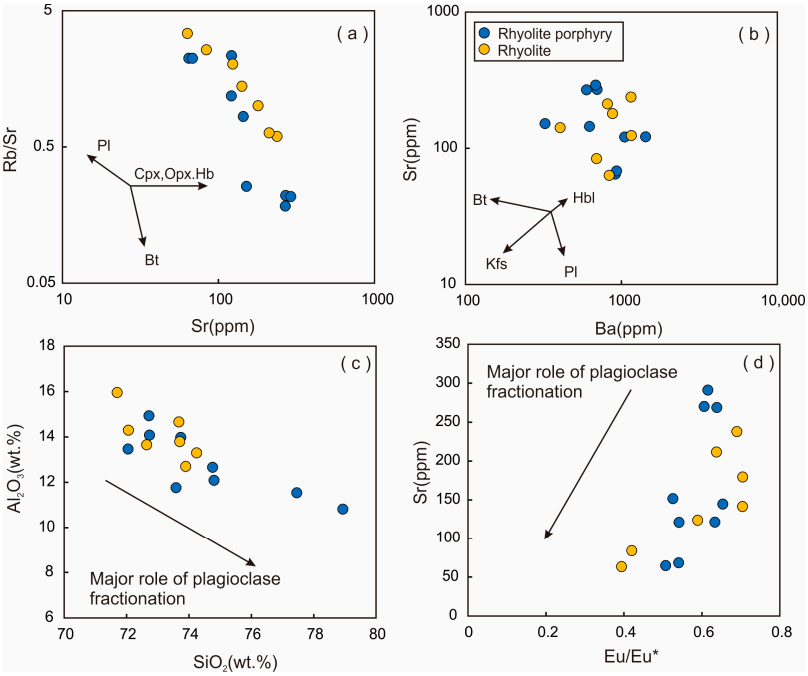



**Figure 10.** Selected major and trace element diagrams of the Hongshuichuan volcanics showing fractionation trends of major and accessory mineral phases. (**a**) Sr versus Rb/Sr; (**b**) Ba versus Sr; (**c**) $SiO_2$ versus $Al_2O_3$; and (**d**) Eu/Eu* versus Sr.

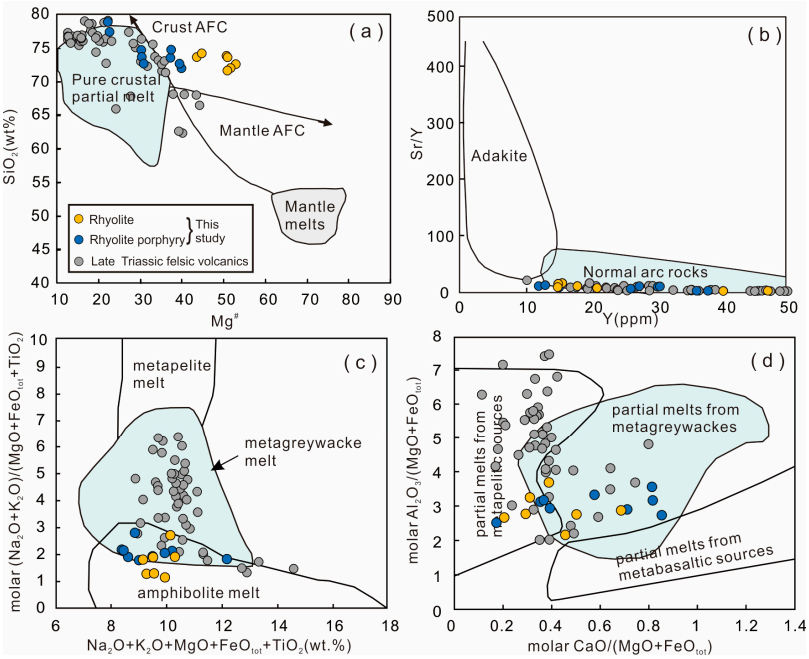



**Figure 11.** (**a**) $Mg^{\#}$ versus $SiO_2$ (after [53,54]); (**b**) Y versus Sr/Y (after [55]); and (**c**,**d**) chemical composition of the studied volcanics. Data sources: [11,16,17,40,56–62] and our unpublished results.

Similarly, the relatively high ratios of $Al_2O_3/(FeO_{tot} + MgO)$ and $CaO/(MgO + FeO_{tot})$ suggest that the studied rhyolite is mainly derived from a metagreywacke source (Figure 11c,d). However, the rhyolite has high contents of $SiO_2$ (71.7–74.3 wt%) and high values of $Mg^{\#}$ (43–53). This, as well as their juvenile or depleted zircon Lu-Hf isotopes, suggests that mantle materials, rather than pure crustal melts, contributed to their origins (Figure 11a). The $\varepsilon Hf(t)$ values of zircons from the rhyolite (−0.6 to 3.0) are much higher than the Triassic granitoids derived from ancient continental crust in the EKOB (average

εHf(t) values of −5.5; [62,63]) but close to the rocks derived from the enriched mantle or crust–mantle magma mixing, further indicating a significant contribution of mantle melts probably derived from the enriched lithospheric mantle (Figure 8). Petrographic studies show that most plagioclase phenocrysts in rhyolite exhibit zoning texture, which is contrasted to the rhyolite porphyry. The widespread presence of zoning textures of plagioclase phenocryst in volcanic rocks is commonly due to the magma mixing between mafic and felsic magmas in open magma systems [63,64].

The rhyolites have similar Hf isotopic compositions with Early Triassic mafic rocks derived from enriched mantle in East Kunlun. (~240Ma gabbro:εHf(t) = −1.8–−0.6 [44]), indicating a significant addition of mantle material probably derived from enriched lithospheric mantle. Rhyolites are LILE enriched and HFSE depleted and show obvious Nb–Ta–Ti troughs in primitive mantle-normalized trace element variation diagrams, exhibiting geochemical features of arc-related magmas, which implies an enrichment mechanism that was related to subducted components. The relative enrichments of Rb, Th, Ta, and Ba (Figure 7), and the obvious depletion in Yb and Y, indicate that mantle below a continental arc, enriched in fluid, could account for these geochemical features. Therefore, mantle-derived magma comes from an enriched lithospheric mantle source that had been metasomatized by subduction-related fluids.

Thus, we propose that the studied rhyolite was derived from the melting of Mesoproterozoic metagraywacke in the lower continental crust with significant involvement of enriched lithospheric mantle -derived magma.

### *6.3. Fractional Crystallization*

The rhyolite porphyry and rhyolite display typical geochemical characteristics of high silica rhyolite with extremely high $SiO_2$ contents (>70 wt%; [65]), thus suggesting that the magma has undergone significant evolution. Fractional crystallization during magma evolution is attested by the marked depletions concerning Ba, Nb, Sr, P, Ti, and Eu on the trace and REE distribution diagrams (Figure 7). Negative Nb-Ti anomalies mirror fractionation of titanium-bearing phases, such as ilmenite or titanite, while negative P anomalies are consistent with apatite fractionation, as also evident by the negative relationship with $P_2O_5$ and $SiO_2$. Plagioclase fractionation is demonstrated by the negative correlation between $SiO_2$ and $Al_2O_3$ (Figure 10c). Plagioclase is an Al-rich mineral; when it is removed from melt, the magma is depleted in $Al_2O_3$.These scenarios explain the pronounced negative Eu anomalies (Figure 9b) because $Ca^{2+}$ is substituted by $Eu^{2+}$ in plagioclase [66]. A decrease in $Al_2O_3$ as a function of plagioclase separation has been proven experimentally [67]. The linear relationship in (Figure 10c,d) further demonstrates the separation of plagioclase during magma evolution.

Zircon geochemistry may allow for a clear picture of magma evolutionary processes [68]. Zircon from the studied rhyolite and rhyolite porphyry exhibit a significant fractionation trend in U/Yb vs. Eu/Eu* diagram (Figure 5d). The Eu/Eu* ratios negatively correlate with Hf (Figure 5c), which can be explained by the crystallization of plagioclase. The diverse zircon compositions along the observed evolutionary path thus reflect amphibole, apatite, and/or titanite fractionation (Figure 5b).

### *6.4. Geodynamic Implications*

Recently, Paleozoic ophiolites with ages of ca. 355–308 Ma have been identified in the East Kunlun Paleo-Tethyan oceanic suture zone, indicating the opening of the Tethyan ocean not later than Carboniferous [69–72]. The regional angular unconformity between the Upper Permian Gequ Formation and the Upper Carboniferous Haoteluowa Formation in the EKOB indicates the occurrence of regional tectonic disturbance during the Late Permian [3]. This regional angular unconformity, as well as the gradually developed Late Permian magmatic rocks with arc-like geochemical affinities, indicates that the Kunlun Paleo-Tethyan oceanic subduction in the EKOB initiated at Late Permian [25,73,74]. However, the subduction duration and the closure time of the Paleo-Tethyan Ocean remain

poorly constrained, which restricts our understanding of the Early Triassic magmatism and tectonics in the EKOB.

The low Sr/Y (1.59–15.5) and La/Yb (8.38–25.7) ratios as well as high Th/Yb ratios (3.76–14.8) and elevated Yb and Y content suggests that the studied Early Triassic felsic volcanic rocks were derived from a normal arc-related magmatic source (Figure 11b, [75]). The studied felsic volcanics are enriched in LILE and depleted in HFSE with negative Nb, Ta, P, and Ti anomalies (Figure 7b), showing affinity to arc-related magmatism. The felsic volcanics plot in the field of volcanic arc granitoids (VAG) in the Ta vs. Yb, Rb vs. (Y + Ta), Rb vs. (Y + Nb), and Nb vs. Y diagrams (Figure 12) further indicate their derivation in a subduction arc setting. The conclusion of the Early Triassic subduction arc setting is consistent with other geological evidence, including the Early Triassic arc-related adakitic quartz diorites and granodiorites (U-Pb age, ca. 243 Ma; [14]) and the subduction-related I-type granites (ca. 244–240 Ma; [44,76]).

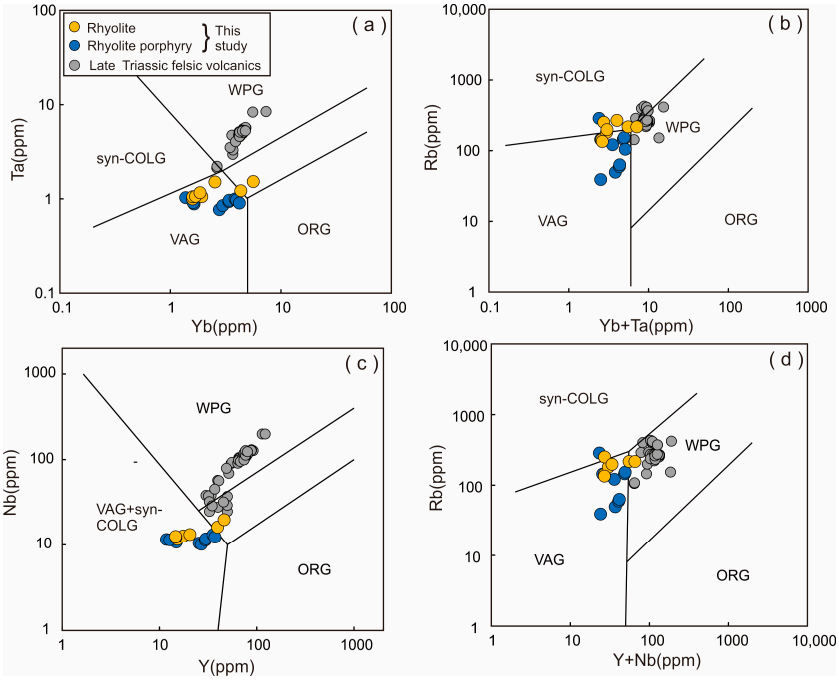



**Figure 12.** Tectonic discrimination diagrams for the studied felsic volcanic rocks (after [77]). (**a**) Yb versus Ta; (**b**) Yb+Ta versus Rb; (**c**) Y versus Nb; (**d**) Y+Nb versus Rb. Data sources: [11,16,17,40] and our unpublished results. ORG, ocean ridge granite; VAG, volcanic arc granite; WPB, within-plate granite; syn-COLG, syn-collisional granite.

The above conclusion is also supported by stratigraphic evidence. Previous studies on the sedimentary strata in the EKOB show that the Late Permian Gequ Formation comprises conglomerate, sandstone, and calcilutite; the Early Triassic Hongshuichuan Formation is mainly composed of bioclastic limestone, lavas, and pyroclastic rocks; and the Middle Triassic Naocangjiangou Formation is mainly composed of sandstone and limestone [3,78,79]. The studies on sedimentary stratigraphy suggest that these Late Permian to Middle Triassic strata containing marine sedimentary rocks all crop out along the southern margin of the proposed East Kunlun continental magmatic arc and are originally deposited in a forearc basin [78,79], recording the northward subduction of the East Kunlun Paleo-Tethyan Ocean. The Late Triassic sedimentary strata are composed of continental volcanic rocks and clastic rocks and are unconformably overlaid on the Late Permian to Middle Triassic strata [3,11,80], representing the closure of the East Kunlun Paleo-Tethyan Ocean and the following continental collision. The studied rhyolite porphyry and rhyolite are geochemically distinct from Late Triassic volcanic rocks in the EKOB, because Late Triassic volcanics have chemical affinity similar to typical within-plate rather than arc-

related rocks (Figure 12, [11,16,17]). Zhu et al. [16] and Shao et al. [17] propose that the Late Triassic volcanic rocks were more likely to generate in a within-plate extension setting. Thus, we propose that the East Kunlun Paleo-Tethyan Ocean subducted northward beneath the East Kunlun-Qaidam terrane during Late Permian-Middle Triassic.

The geochemical and zircon Lu-Hf isotopic studies show that the studied rhyolite porphyry and rhyolite originated from the melting of pure ancient continental crust, but the origin of the latter one has a certain contribution of crust–mantle magma mixing. Therefore, the reworking of the ancient continental lithosphere and magma mixing are important mechanisms for continental crust growth. In summary, we propose a tectonic and crustal evolution model for the EKOB during Early Triassic (Figure 13). Owing to the sinking slab of the Kunlun Paleo-Tethyan oceanic crust and lithospheric mantle during the Early Triassic, the melting of the metasomatized mantle wedge generated the mafic magma. The following underplating of the mafic magma heated the lower continental crust and triggered its melting to form the felsic magma. The felsic magma underwent fractionation and then directly erupted upward to form low-Mg$^{\#}$ felsic volcanic rocks (i.e., rhyolite porphyry) with enriched zircon Hf isotopic compositions, while some felsic magmas mixed with mantle-derived mafic magmas to form high-Mg$^{\#}$ felsic rocks (i.e., rhyolite) with plagioclase zoning and depleted zircon Hf isotopes.

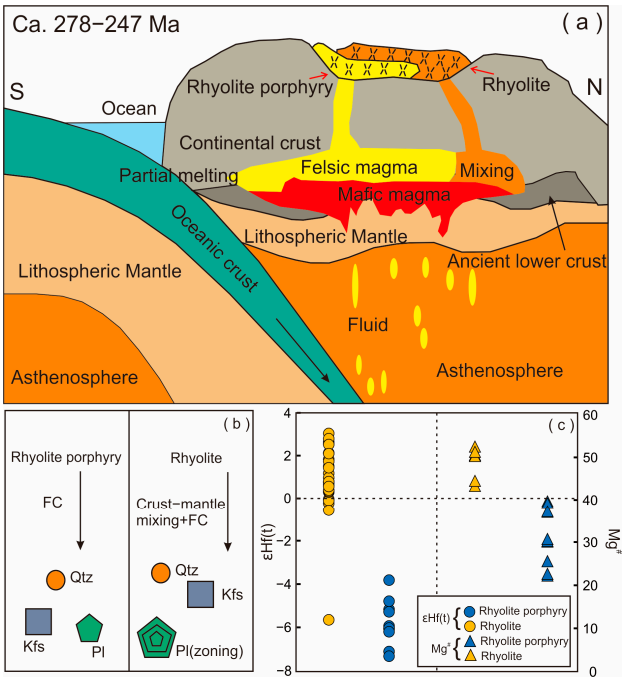



**Figure 13.** (**a**) Schematic cartoons showing the tectonic magmatic evolution of the Early Triassic igneous rocks in the EKOB; (**b**) Schematic diagram of the genesis of rhyolite and rhyolite porphyry; (**c**) Zircon εHf(t) and Mg$^{\#}$ value distribution of the studied felsic volcanic rocks.

## 7. Conclusions

1. The studied rhyolite and rhyolite porphyry in the Hongshuichuan Formation from the East Kunlun orogenic belt, North Tibet, are synchronously formed in Early Triassic (ca. 251–247 Ma).
2. Elemental and isotopic geochemistry studies indicate that the rhyolite porphyry and rhyolite have typical lower crust-derived characteristics, and they are generated by partial melting of Mesoproterozoic metagreywacke sources with a certain amount of mantle-derived mafic magmas involved in the origin of the high Mg$^{\#}$ rhyolite.
3. The studied ca. 250 Ma felsic volcanic rocks were formed during the northward subduction of the East Kunlun Paleo-Tethyan oceanic slab. This study suggests

that the reworking of ancient continental crust and crust–mantle magma mixing are important mechanisms for the evolution of the orogenic continental crust.

**Supplementary Materials:** The following supporting information can be downloaded at: https://www.mdpi.com/article/10.3390/min13050607/s1, Table S1: LA-ICP-MS zircon U-Pb data for the studied Early Triassic felsic volcanic rocks in the EKOB; Table S2: Zircon trace elements for the studied Early Triassic felsic volcanic rocks in the EKOB; Table S3: Whole-rock major and trace element compositions of the studied Early Triassic felsic volcanic rocks in the EKOB; Table S4 Zircon Lu-Hf isotopes for the studied Early Triassic felsic volcanic rocks in the EKOB.

**Author Contributions:** Conceptualization, D.Y. and F.X.; Interpretation of data, Z.C.; Methodology, Z.L.; Analysis of data, W.W.; Writing—original draft preparation, D.Y. and Z.C.; Writing—review and editing, D.Y. and F.X.; Funding acquisition, F.X. All authors have read and agreed to the published version of the manuscript.

**Funding:** This study was financially supported by the National Natural Science Foundation of China (No. 41602049) and the Research Project of Chengdu University of Technology (No. 2022ZF11412).

**Data Availability Statement:** The original contributions presented in the study are included in the article/Supplementary Material.

**Acknowledgments:** We sincerely thank the journal editor and three anonymous reviewers for their constructive comments and suggestions, which substantially improved our manuscript.

**Conflicts of Interest:** The authors declare no conflict of interest.

## References

1. Chen, G.C.; Pei, X.Z.; Li, R.; Li, Z.C.; Pei, L.; Liu, C.J.; Chen, Y.X.; Wang, M. Late Paleozoic-Early Mesozoic tectonic-magmatic evolution and mineralization in the eastern section of the East Kunlun Orogenic Belt. *Acta Geol. Sin. (Engl. Ed.)* **2019**, *93*, 158–159.
2. Dong, Y.P.; He, D.F.; Sun, S.S.; Liu, X.M.; Zhou, X.H.; Zhang, F.F.; Yang, Z.; Cheng, B.; Zhao, G.C.; Li, J.H. Subduction and accretionary tectonics of the East Kunlun orogen, western segment of the Central China Orogenic System. *Earth Sci. Rev.* **2018**, *186*, 231–261. [CrossRef]
3. Li, R.B.; Pei, X.Z.; Li, Z.C.; Liu, Z.Q.; Chen, G.C.; Chen, Y.X.; Wei, F.H.; Gao, J.M.; Liu, C.J.; Pei, L. Geological characteristics of Late Paleozoic-Mesozoic unconformities and their response to some significant tectonic events in eastern part of Eastern Kunlun. *Earth Sci. Front.* **2012**, *19*, 244–254, (In Chinese with English Abstract).
4. Shao, F.L.; Niu, Y.L.; Regelous, M.; Zhu, D.C. Petrogenesis of peralkaline rhyolites in an intra-plate setting: Glass House Mountains, southeast Queensland, Australia. *Lithos* **2015**, *216*, 196–210. [CrossRef]
5. Tian, W.; Campbell, I.H.; Allen, C.M.; Guan, P.; Pan, W.Q.; Chen, M.M.; Yu, H.J.; Zhu, W.P. The Tarim picrite–basalt–rhyolite suite, a Permian flood basalt from northwest China with contrasting rhyolites produced by fractional crystallization and anatexis. *Contrib. Mineral. Petrol.* **2010**, *160*, 407–425. [CrossRef]
6. Ratajeski, K.; Glazner, A.F.; Miller, B.V. Geology and geochemistry of mafic to felsic plutonic rocks in the Cretaceous intrusive suite of Yosemite Valley, California. *Geol. Soc. Am. Bull.* **2001**, *113*, 1486–1502. [CrossRef]
7. Takanashi, K.; Shuto, K.; Sato, M. Origin of Late Paleogene to Neogene basalts and associated coeval felsic volcanic rocks in Southwest Hokkaido, northern NE Japan arc: Constraints from Sr and Nd isotopes and major- and trace-element chemistry. *Lithos* **2011**, *125*, 368–392. [CrossRef]
8. Lu, S.Y.; Ren, Y.S.; Hou, H.N.; Li, J.M.; Hao, Y.J.; Shang, Q.Q. Petrogenesis, tectonic setting, and metallogenic significance of the Middle Permian volcanic rock system of the Miaoling Formation, Yanbian area, NE China: Constraints from geochronology, geochemistry, and Sr–Nd–Hf isotopes. *Geochemistry* **2022**, *82*, 125902. [CrossRef]
9. Gogoi, B.; Saikia, A.; Ahmad, M. Field evidence, mineral chemical and geochemical constraints on mafic-felsic magma interactions in a vertically zoned magma chamber from the Chotanagpur Granite Gneiss Complex of Eastern India. *Geochemistry* **2018**, *78*, 78–102. [CrossRef]
10. Gogoi, B.; Chauhan, H.; Saikia, A. Understanding mafic-felsic magma interactions in a subvolcanic magma chamber using rapakivi feldspar: A case study from the Bathani volcano-sedimentary sequence, eastern India. *Geochemistry* **2021**, *81*, 125730. [CrossRef]
11. Yan, H.; Niu, Y.L.; Li, J.Y.; Lei, Y.; Kong, J.J.; Chen, S.; Zhang, Y.; Zhang, G.R. Petrogenesis and tectonic significance of the late Triassic mafic dikes and felsic volcanic rocks in the East Kunlun Orogenic Belt, Northern Tibet Plateau. *Lithos* **2016**, *245*, 205–222.
12. Yang, J.H.; Wu, F.Y.; Wilde, S.A.; Chen, F.K.; Liu, X.M.; Xie, L.W. Petrogenesis of an alkali syenite–granite–rhyolite suite in the Yanshan fold and thrust belt, Eastern North China Craton: Geochronological, geochemical and Nd–Sr–Hf isotopic evidence for lithospheric thinning. *J. Petrol.* **2008**, *49*, 315–351. [CrossRef]

13. Huang, H.; Niu, Y.; Nowell, G.; Zhao, Z.; Yu, X.; Zhu, D.C. Geochemical Constraints on the Petrogenesis of Granitoids in the East Kunlun Orogenic Belt, Northern Tibetan Plateau: Implications for Continental Crust Growth through Syn-Collisional Felsic Magmatism. *Chem. Geol.* **2014**, *370*, 1–18. [CrossRef]
14. Xiong, F.H.; Ma, C.Q.; Zhang, J.Y.; Liu, B.; Jiang, H.A. Reworking of old continental lithosphere: An important crustal evolution mechanism in orogenic belts, as evidenced by Triassic I-type granitoids in the East Kunlun orogen, Northern Tibetan Plateau. *J. Geol. Soc.* **2014**, *171*, 847–863. [CrossRef]
15. Li, X.W.; Huang, X.F.; Luo, M.F.; Dong, G.C.; Mo, X.X. Petrogenesis and geodynamic implications of the Mid-Triassic lavas from East Kunlun, northern Tibetan Plateau. *J. Asian Earth Sci.* **2015**, *105*, 32–47. [CrossRef]
16. Zhu, Y.X.; Wang, L.X.; Ma, C.Q.; He, Z.X.; Deng, X.; Tian, Y. Petrogenesis and tectonic implication of the Late Triassic A1-type alkaline volcanics from the Xiangride area, eastern segment of the East Kunlun Orogen (China). *Lithos* **2022**, *412–413*, 106595. [CrossRef]
17. Shao, F.L.; Niu, Y.L.; Kong, J.J.; Liu, Y.; Wang, G.D.; Zhang, Y. Petrogenesis and tectonic implications of the Triassic rhyolites in the East Kunlun Orogenic Belt, northern Tibetan Plateau. *Geosci. Front.* **2021**, *12*, 101243. [CrossRef]
18. Xiong, F.H.; Ma, C.Q.; Jiang, H.A.; Liu, B.; Huang, J. Geochronology and geochemistry of Middle Devonian mafic dykes in the East Kunlun orogenic belt, Northern Tibet Plateau: Implications for the transition from Prototethys to Paleotethys orogeny. *Geochemistry* **2014**, *74*, 225–235. [CrossRef]
19. Chen, G.C.; Pei, X.Z.; Li, R.B.; Li, Z.C.; Chen, Y.X.; Liu, C.J.; Pei, L. Multiple Sources of Indosinian Granites and Constraints on the Tectonic Evolution of the Paleo-Tethys Ocean in East Kunlun Orogen. *Minerals* **2022**, *12*, 1604. [CrossRef]
20. Xia, R.; Wang, C.M.; Qing, M.; Li, W.L.; Carranza, E.J.M.; Guo, X.D.; Ge, L.S.; Zeng, G.Z. Zircon U-Pb dating, geochemistry and Sr–Nd–Pb–Hf–O isotopes for the Nan'getan granodiorites and mafic microgranular enclaves in the East Kunlun Orogen: Record of closure of the Paleo-Tethys. *Lithos* **2015**, *234–235*, 47–60. [CrossRef]
21. Shao, F.L.; Niu, Y.L.; Liu, Y.; Chen, S.; Kong, J.J.; Duan, M. Petrogenesis of Triassic granitoids in the East Kunlun Orogenic Belt, northern Tibetan Plateau and their tectonic implications. *Lithos* **2017**, *282*, 33–44. [CrossRef]
22. Ren, H.D.; Wang, T.; Zhang, L.; Wang, X.X.; Huang, H.; Feng, C.Y.; Teschner, C.; Song, P. Ages, sources and tectonic settings of the triassic igneous rocks in the easternmost Segment of the East Kunlun Orogen, Central China. *Acta Geol. Sin. (Engl. Ed.)* **2016**, *90*, 641–668.
23. Roger, F.; Jolivet, M.; Malavieille, J. Tectonic evolution of the Triassic fold belts of Tibet. *Compt. Rendus Geosci.* **2008**, *340*, 180–189. [CrossRef]
24. Jiang, C.F.; Yang, J.S.; Feng, B.G.; Zhu, Z.Z.; Zhao, M.; Chai, Y.C.; Shi, X.D.; Wang, H.D.; Hu, J.Q. Opening–closing tectonics of Kunlun Mountains. *Ser. Geol. Mem.* **1992**, *5*, 1–224, (In Chinese with English Abstract).
25. Liu, B.; Ma, C.Q.; Zhang, J.Y.; Xiong, F.H.; Huang, J.; Jiang, H.A. 40Ar–39Ar age and geochemistry of subduction-related mafic dikes in northern Tibet, China: Petrogenesis and tectonic implications. *Int. Geol. Rev.* **2014**, *56*, 57–73. [CrossRef]
26. Mo, X.X.; Luo, Z.H.; Deng, J.F.; Yu, X.H.; Liu, C.D.; Chen, H.W.; Yuan, W.M.; Liu, Y.H. Granitoids and crustal growth in the East-Kunlun Orogenic Belt. *Geol. J. China Univ.* **2007**, *13*, 403–414, (In Chinese with English Abstract).
27. Ren, J.H.; Liu, Y.Q.; Zhou, D.W.; Feng, Q.; Zhang, K.; Dong, Z.L.; Qin, P.L. Geochemical characteristics and LA-ICP-MS zircon U–Pb dating of basic dykes in the Xiaomiao area, East Kunlun. *J. Jilin Univ. (Earth Sci. Ed.)* **2010**, *40*, 859–868, (In Chinese with English Abstract).
28. Ludwig, K.R. *User's Manual for Isoplot/ex Version 3.00: A Geochronological Toolkit for Microsoft Excel*; Special Publication; Berkeley Geochronology Center: Berkeley, CA, USA, 2003.
29. Liu, Y.; Gao, S.; Hu, Z.; Gao, C.; Zong, K.; Wang, D. Continental and oceanic crust recycling-induced melt–peridotite interactions in the Trans-North China Orogen: U–Pb dating, Hf isotopes and trace elements in zircons from mantle xenoliths. *J. Petrol.* **2010**, *51*, 537–571. [CrossRef]
30. Ma, Q.; Zheng, J.; Griffin, W.L.; Zhang, M.; Tang, H.; Su, Y.; Ping, X. Triassic "adakitic" rocks in an extensional setting (North China): Melts from the cratonic lower crust. *Lithos* **2012**, *149*, 159–173. [CrossRef]
31. Liu, Y.; Hu, Z.; Gao, S.; Günther, D.; Xu, J.; Gao, C. In Situ Analysis of Major and Trace Elements of Anhydrous Minerals by La-Icp-Ms without Applying an Internal Standard. *Chem. Geol.* **2008**, *257*, 34–43. [CrossRef]
32. Hu, Z.; Liu, Y.; Gao, S.; Liu, W.; Zhang, W.; Tong, X.; Lin, L.; Zong, K.; Li, M.; Chen, H.; et al. Improved in situ Hf isotope ratio analysis of zircon using newly designed X skimmer cone and jet sample cone in combination with the addition of nitrogen by laser ablation multiple collector ICP-MS. *J. Anal. At. Spectrom.* **2012**, *27*, 1391–1399. [CrossRef]
33. Belousova, E.A.; Griffin, W.L.; O'Reilly, S.Y. Zircon crystal morphology, trace element signatures and Hf isotope composition as a tool for petrogenetic modelling: Examples from Eastern Australian granitoids. *J. Petrol.* **2006**, *47*, 329–353. [CrossRef]
34. Zhu, Y.X.; Wang, L.X.; Ma, C.Q.; Wiedenbeck, M.; Wang, W. The Neoproterozoic alkaline rocks from Fangcheng area, East Qinling (China) and their implications for regional Nb mineralization and tectonic evolution. *Precambrian Res.* **2020**, *350*, 105852. [CrossRef]
35. Middlemost, E.A.K. Naming materials in the magma/igneous rock system. *Earth-Sci. Rev.* **1994**, *37*, 215–224. [CrossRef]
36. Peccerillo, A.; Taylor, S.R. Geochemistry of Eocene calc-alkaline volcanic rocks from the Kastamonu area, northern Turkey. *Contrib. Mineral. Petrol.* **1976**, *58*, 63–81. [CrossRef]
37. Frost, C.D.; Frost, B.R. On ferroan (A-type) granitoids: Their compositional variability and modes of origin. *J. Petrol.* **2010**, *52*, 39–53. [CrossRef]

38. Sun, S.S.; McDonough, W.F. Chemical and isotopic systematics of oceanic basalts:implications for mantle composition and processes. In *Magmatism in the Ocean Basins*; Saunders, A.D., Norry, M.J., Eds.; Special Publications; Geological Society: London, UK, 1989; Volume 42, pp. 313–345.
39. Taylor, S.R.; McLennan, S.M. *The Continental Crust: Its Composition and Evolution*; Oxford Press: Blackwell, UK, 1985; pp. 1–312.
40. Ding, S.; Huang, H.; Niu, Y.L.; Zhao, Z.D.; Yu, X.H.; Mo, X.X. Geochemistry, geochronology and petrogenesis of East Kunlun high Nb-Ta rhyolites. *Acta Petrol. Sin.* **2011**, *27*, 3603–3614, (In Chinese with English Abstract).
41. Wei, X.; Sun, F.Y.; Zhang, Y.T.; Fan, X.Z.; Wang, Y.C.; Li, L. Mafic–intermediate igneous rocks in the East Kunlun Orogenic Belt, northwestern China: Petrogenesis and implications for regional geodynamic evolution during the Triassic. *Lithos* **2019**, *346–347*, 105159.
42. Kamaunji, V.D.; Wang, L.X.; Ma, C.Q.; Liu, J.; Zhu, Y.X. Petrogenesis and tectonic implication of the Permian-Triassic syenogranites from the eastern segment of the East Kunlun Orogen, China. *Lithos* **2020**, *25*, 105932. [CrossRef]
43. Kong, J.J.; Niu, Y.L.; Hu, Y.; Zhang, Y.; Shao, F.L. Petrogenesis of the Triassic granitoids from the East Kunlun Orogenic Belt, NW China: Implications for continental crust growth from syn-collisional to post-collisional setting. *Lithos* **2020**, *364–365*, 105513. [CrossRef]
44. Yan, D.D.; Xiong, F.H.; Ma, C.Q.; Hou, M.C.; Zhao, H. Petrogenesis of Middle Triassic intermediate-mafic igneous rocks in East Kunlun, Northern Tibet: Implications for the crust growth and Paleo-Tethyan orogeny. *Geosyst. Geoenviron.* **2022**, 100096. [CrossRef]
45. Song, Z.T.; Xu, X.S. Petrogenesis of high-maficity S-type granites: Insight from the early Paleozoic Jinxi granite, South China. *Lithos* **2022**, *106597*, 412–413. [CrossRef]
46. Whalen, J.B.; Currie, K.L.; Chappell, B.W. A-type granites; geochemical characteristics, discrimination and petrogenesis. *Contrib. Mineral. Petrol.* **1987**, *95*, 407–419. [CrossRef]
47. Chen, S.W.; Li, J.H.; Yuan, F.; Li, L.M.; Deng, Y.F.; Jowitt, S.M.; Jiang, R.; Li, Z.W.; Yuan, F.; Li, Y.; et al. Geochemistry and geochronology of I–type granites of the Feidong Complex, eastern China: Implications for the Paleoproterozoic tectonic evolution of the Yangtze Craton. *Precambrian Res.* **2022**, *382*, 106884. [CrossRef]
48. Jiang, X.Y.; Luo, J.C.; Guo, J.; Wu, K.; Zhang, Z.K.; Sun, W.D.; Xia, X.P. Geochemistry of I- and A-type granites of the Qingyang–Jiuhuashan complex, eastern China: Insights into early cretaceous multistage magmatism. *Lithos* **2018**, *316–317*, 278–294. [CrossRef]
49. Yokoyama, T.; Okumura, S.; Nakashima, S. Hydration of rhyolitic glass during weathering as characterized by IR microspectroscopy. *Geochim. Cosmochim. Acta* **2008**, *72*, 117–125. [CrossRef]
50. Shellnutt, G.J.; Wang, C.Y.; Zhou, M.F.; Yang, Y. Zircon Lu–Hf isotopic compositions of metaluminous and peralkaline A-type granitic plutons of the Emeishan large igneous province (SW China): Constraints on the mantle source. *J. Asian Earth Sci.* **2009**, *35*, 45–55. [CrossRef]
51. Green, T.H. Significance of Nb/Ta as an indicator of geochemical processes in the crust-mantle system. *Chem. Geol.* **1995**, *120*, 347–359. [CrossRef]
52. Weaver, B.L. The origin of ocean island basalt end member compositions: Trace element and isotopic constrains. *Earth Planet. Sci. Lett.* **1991**, *104*, 381–397. [CrossRef]
53. Patiño Douce, A.E.; Johnston, A.D. Phase equilibria and melt productivity in the pelitic system: Implications for the origin of peraluminous granitoids and aluminous granulites. *Contrib. Mineral. Petrol.* **1991**, *107*, 202–218. [CrossRef]
54. Rapp, R.P.; Watson, E.B. Dehydration melting of metabasalt at 8–32 kbar: Implications for continental growth and crust–mantle recycling. *J. Petrol.* **1995**, *36*, 891–931. [CrossRef]
55. Castillo, P.R. Origin of the adakite high-Nb basalt association and its implications for postsubduction magmatism in Baja California, Mexico. *Geol. Soc. Am. Bull.* **2008**, *120*, 451–462. [CrossRef]
56. Vielzeuf, D.; Holloway, J.R. Experimental determination of the fluid-absent melting relations in the pelitic system. *Contrib. Mineral. Petrol.* **1988**, *98*, 257–276. [CrossRef]
57. Rapp, R.P.; Watson, E.B.; Miller, C.F. Partial melting of amphibolite/eclogite and the origin of Archean trondhjemites and tonalites. *Precambrian Res.* **1991**, *51*, 1–25. [CrossRef]
58. Gardien, V.; Thompson, A.B.; Grujic, D.; Ulmer, P. Experimental melting of biotite + plagioclase + quartz ± muscovite assemblages and implications for crustal melting. *J. Geophys. Res.* **1995**, *100*, 15581–15591. [CrossRef]
59. Patiño Douce, A.E.; Beard, J.S. Effects of P, f(O2) and Mg/Fe ratio on dehydration melting of model metagreywackes. *J. Petrol.* **1996**, *37*, 999–1024. [CrossRef]
60. Skjerlie, K.P.; Johnston, A.D. Vapour-absent melting from 10 to 20 kbar of crustal rocks that contain multiple hydrous phases: Implications for anatexis in the deep to very deep continental crust and active continental margins. *J. Petrol.* **1996**, *37*, 661–691. [CrossRef]
61. Patiño Douce, A.E. Generation of metaluminous A-type granites by low-pressure melting of calc-alkaline granitoids. *Geology* **1997**, *25*, 743–746. [CrossRef]
62. Stevens, G.; Clemens, J.D.; Droop, G.T.R. Melt production during granulite-facies anatexis: Experimental data from 'primitive' metasedimentary protoliths. *Contrib. Mineral. Petrol.* **1997**, *128*, 352–370. [CrossRef]
63. Druitt, T.H.; Costa, F.; Deloule, E.; Dungan, M.; Scaillet, B. Decadal to monthly timescales of magma transfer and reservoir growth at a caldera volcano. *Nature* **2012**, *482*, 77–80. [CrossRef]

64. Xiong, F.H.; Ma, C.Q.; Chen, B.; Ducea, M.N.; Hou, M.C.; Ni, S.J. Intermediate-mafic Dikes in the East Kunlun Orogen, Northern Tibetan Plateau: A Window into Paleo-arc Magma Feeding System. *Lithos* **2019**, *340–341*, 152–165. [CrossRef]
65. Gualda, G.A.R.; Ghiorso, M.S. Low-pressure origin of high-silica rhyolites and granites. *J. Geol.* **2013**, *121*, 537–545. [CrossRef]
66. Vasyukova, O.; Williams-Jones, A. Partial melting, fractional crystallisation, liquid immiscibility and hydrothermal mobilisation—A 'recipe' for the formation of economic A-type granite-hosted HFSE deposits. *Lithos* **2019**, *356–357*, 105300. [CrossRef]
67. Villiger, S.; Müntener, O.; Ulmer, P. Crystallization pressures of mid-ocean ridge basalts derived from major element variations of glasses from equilibrium and fractional crystallization experiments. *J. Geophys. Res. Solid Earth* **2007**, *112*, B01202. [CrossRef]
68. Lee, R.G.; Dilles, J.H.; Tosdal, R.M.; Wooden, J.L.; Mazdab, F.K. Magmatic evolution of granodiorite intrusions at the El Salvador porphyry copper deposit, Chile, based on trace element composition and U/Pb age of zircons. *Econ. Geol.* **2017**, *112*, 245–273. [CrossRef]
69. Chen, L.; Sun, Y.; Pei, X.; Gao, M.; Feng, T.; Zhang, Z.; Chen, W. Northernmost paleo-tethyan oceanic basin in Tibet: Geochronological evidence from 40Ar/39Ar age dating of Dur'ngoi ophiolite. *Chin. Sci. Bull.* **2001**, *46*, 1203–1205. [CrossRef]
70. Bian, Q.T.; Li, D.H.; Pospelov, I.; Yin, L.M.; Li, H.S.; Zhao, D.S.; Chang, C.F.; Luo, X.Q.; Gao, S.L.; Astrakhantsev, O.; et al. Age, geochemistry and tectonic setting of Buqingshan ophiolites, North Qinghai-Tibet Plateau, China. *J. Asian Earth Sci.* **2004**, *23*, 577–596. [CrossRef]
71. Yang, J.S.; Shi, R.D.; Wu, C.L.; Wang, X.B.; Robinson, P. Dur'ngoi ophiolite in East Kunlun, Northeast Tibetan plateau: Evidence for paleo-Tethyan suture in Northwest China. *J. Earth Sci.* **2009**, *20*, 303–331. [CrossRef]
72. Liu, Z.Q.; Pei, X.Z.; Li, R.B.; Li, Z.C.; Zhang, X.F.; Liu, Z.G.; Chen, G.H.; Chen, Y.X.; Ding, S.P.; Guo, J.F. LA-ICP-MS Zircon U-Pb Geochronology of the Two Suites of Ophiolites at the Buqiangshan Area of the A'nyemaqen Orogenic Belt in the Southern Margin of East Kunlun and its tectonic implication. *Acta Geol. Sin.* **2011**, *85*, 185–194.
73. Li, R.B.; Pei, X.Z.; Li, Z.C.; Pei, L.; Chen, G.H.; Liu, Z.Q.; Chen, Y.X.; Liu, C.J.; Wang, M.; Zhang, M. Paleo-Tethyan Ocean Evolution and Indosinian Orogenesis in the East Kunlun Orogen, Northern Tibetan Plateau. *Minerals* **2022**, *12*, 1590. [CrossRef]
74. Xiong, F.H.; Ma, C.Q.; Zhang, J.Y.; Liu, B. The origin of mafic microgranular enclaves and their host granodiorites from East Kunlun, Northern qinghai–Tibet Plateau: Implications for magma mixing during subduction of Paleo-Tethyan lithosphere. *Miner. Petrol.* **2012**, *104*, 211–224. [CrossRef]
75. Martin, H. Adakitic magmas: Modern analogues of Archaean granitoids. *Lithos* **1999**, *46*, 411–429. [CrossRef]
76. Li, R.B.; Pei, X.Z.; Pei, L.; Li, Z.C.; Chen, G.C.; Chen, Y.X.; Liu, C.J.; Wang, M. The Early Triassic Andean-type Halagatu granitoids pluton in the East Kunlun orogen, northern Tibet Plateau: Response to the northward subduction of the Paleo-Tethys Ocean. *Gondwana Res.* **2018**, *62*, 212–226. [CrossRef]
77. Pearce, J.A.; Harris, N.; Tindle, A.G. Trace element discrimination diagrams for the tectonic interpretation of granitic rocks. *J. Petrol.* **1984**, *25*, 956–983. [CrossRef]
78. Yan, Z.; Bian, Q.T.; Korchagin, O.A.; Pospelov, I.I.; Li, J.L.; Wang, Z.Q. Provenance of Early Triassic Hongshuichuan formation in the southern margin of the East Kunlun Mountains: Constrains from detrial framework, heavy mineral analysis and geochem istry. *Acta Petrol. Sin.* **2008**, *24*, 1068–1078, (In Chinese with English Abstract).
79. Yue, Y.G.; Dong, Y.P.; Sun, S.S.; He, D.F. Mafic-ultramafic rocks in the Buqingshan Complex of the East Kunlun Orogen, northern Tibetan Plateau: Remnants of the Paleo-Tethys Ocean. *Int. Geol. Rev.* **2022**, *64*, 3149–3170. [CrossRef]
80. Fan, X.Z.; Sun, F.Y.; Xu, C.H.; Wu, Q.Q.; Yu, L.; Wang, L.; Yan, C.; Bakht, S. Volcanic rocks of the Elashan Formation in the Dulan-Xiangride Basin, East Kunlun Orogenic Belt, NW China: Petrogenesis and implications for Late Triassic geodynamic evolution. *Int. Geol. Rev.* **2021**, *64*, 1270–1293. [CrossRef]


**Disclaimer/Publisher's Note:** The statements, opinions and data contained in all publications are solely those of the individual author(s) and contributor(s) and not of MDPI and/or the editor(s). MDPI and/or the editor(s) disclaim responsibility for any injury to people or property resulting from any ideas, methods, instructions or products referred to in the content.